

See discussions, stats, and author profiles for this publication at: <https://www.researchgate.net/publication/338979985>

# Estimating the hydraulic profiles in a cross-section under one-dimensional steady-flow dynamics by employing the entropy maximization principle: II. Applications

Preprint · November 2019

CITATION

1

READS

177

4 authors:



**Panayiotis Dimitriadis**

National Technical University of Athens

138 PUBLICATIONS 754 CITATIONS

[SEE PROFILE](#)



**Evangelos Rozos**

National Observatory of Athens

64 PUBLICATIONS 759 CITATIONS

[SEE PROFILE](#)



**Katerina Mazi**

National Observatory of Athens

36 PUBLICATIONS 513 CITATIONS

[SEE PROFILE](#)



**Antonis D. Koussis**

National Observatory of Athens

152 PUBLICATIONS 1,869 CITATIONS

[SEE PROFILE](#)

Some of the authors of this publication are also working on these related projects:



The uncertainty of atmospheric processes in planning a hybrid renewable energy system for a non-connected island [View project](#)



Sub surface flow in sloping aquifers [View project](#)

# Estimating the hydraulic profiles in a cross-section under one-dimensional steady-flow dynamics by employing the entropy maximization principle: II. Applications

Panayiotis Dimitriadis<sup>\*1</sup>, Evangelos Rozos<sup>1</sup>, Katerina Mazi<sup>1</sup>, Antonis D. Koussis<sup>1</sup>, and Demetris Koutsoyiannis<sup>2</sup>

<sup>1</sup>Institute for Environmental Research and Sustainable Development, National Observatory of Athens

<sup>\*</sup>corresponding author; email: pandim@itia.ntua.gr

## Abstract

We apply the revisited maximum-entropy framework developed in Dimitriadis et al. (2019b), where theoretical profiles for the longitudinal velocity, pressure and water-depth in a cross-sections under one-dimensional steady flow dynamics are derived. The maximum entropy distribution is applied to each variable of interest-based on the number of moments conserved through the 1d conservation of mass, linear momentum and energy. This distribution is then combined with the distribution of sampling location, which for convenience is assumed uniform, to express the absolute derivative of the variable of interest with respect to location. Through several applications, we show that the above configuration exhibits advantages compared to the established analysis, such as the flexibility to conserve additional moments, to derive not only the typical von Kàrman but also alternative profiles, the implicit construction of the dip-phenomenon, and the streamflow estimation under reasonable assumptions for the shear stress. We further illustrate how the assumed uniform distribution for the location variable can be regarded as the spatial sampling distribution in a cross-section. A limitation of the proposed framework is that the derived profiles can be sometimes complicated and, so, they can be simulated only numerically. Regarding the sampling strategy, we discuss how the choice of a uniform distribution of sampling points is also convenient requiring the least effort and information for sampling at a fixed area. Finally, we discuss that even with a few velocity samples we may estimate the streamflow with relatively high accuracy and a small error (in the order of 10%) if only surface velocities are sampled.

*Keywords:* entropy-maximization; 1d steady-flow dynamics; velocity profile; pressure profile; water-depth profile; sampling strategy

## 1. Introduction

In this work we demonstrate, with test applications, the method for estimating the hydraulic profiles in a channel cross-section under one-dimensional steady-flow dynamics presented in the companion paper Dimitriadis et al. (2019b). That entropy-maximization method is embedded in a probabilistic-deterministic framework and uses the absolute values of the original, e.g.  $v = g(s)$ , or transformed to be  $\zeta(s)$ , monotonic first spatial derivative of the longitudinal velocity  $v$  (transversal to the flow), pressure and water-depth in a cross-section as a function of the location variable  $s$ . The applications concern open-channel flow and flow in pipes with prismatic and irregular cross-sections. We reiterate that in open-channel flow the revisited framework does not require knowing the iso-velocity (similarly for the iso-pressure) lines or introducing explicit

parameters for the position and magnitude of the maximum velocity, only values at the boundaries are required, such as surface velocities and total water-depths. As we show, the latter variables can be implicitly estimated through the velocity distribution. In pipe flow, the velocity and pressure positions and magnitudes are required at a single point of the cross-section. Section 2 summarises the results of the analysis in Dimitriadis et al. (2019) that are used in the test cases shown in the applications of section 3. Also, at the end of section 3, we discuss the implications of the proposed framework to the sampling strategy, and we show that the choice of a uniform distribution of sampling points is not only theoretically justified but also convenient requiring the least effort for in-stream recording methods and information for sampling over a fixed area. The above practise is expected to be advantageous compared to the traditional practices especially during flood events. A limitation of the proposed framework is that the derived profiles can be sometimes complicated and therefore, they can be simulated only numerically (see applications in sect. 3). The reader is referred to that companion paper for the analysis itself and for the notation, as well as for the methodology used to derive the velocity, pressure and depth profiles.

## 2. Proposed maximum-entropy probabilistic framework

As shown in Dimitriadis et al. (2019b), the probability distribution for the sampling location (or else sampling position in the cross-section) random variable  $s$  is considered axiomatically as uniform (abbreviated ME0, Table 1). The maximized entropy probability distribution for the pressure  $p$  results in the exponential distribution (abbreviated ME1, Table 1) or when it is important to conserve the pressure centroid, to the lower-tail truncated Gaussian one (abbreviated ME2; Table 1). The water-depth  $w$  is analysed similarly to the pressure (ME1 or ME2), and in cases of a hydrostatic profile the two variables have identical distributions and parameters. The resulting distribution for the velocity  $v$  is the three-parameter maximized entropy distribution (abbreviated ME3; Table 1) that can sometimes be approximated well by a Pareto-Burr-Feller distribution (abbreviated PBF, Table 1). As discussed in Dimitriadis et al. (2019b), all three-variables, i.e. velocity, pressure and waterdepth, may be sometimes (depending on the examined case) approximated well by a simpler version of the distribution derived by applying the entropy maximization principle in the one-dimensional steady-flow dynamics. An illustrative example is the one-dimensional plane Couette flow, where all three variables follow the uniform ME0 distribution.

It is noted that the above distribution may require further truncation in case the values at the boundaries are observed or specified, in order to pass this information on as a constraint for the entropy maximization. It is again stressed that the unobserved or unspecified boundary values are required in the deterministic re-construction model and not in the probabilistic one. After the probability distribution is selected, the profile of the above three variables can be (analytically or numerically) simulated by the change of variable technique (as thoroughly analysed in Dimitriadis et al., 2019b, sect. 2.2). For example, a useful solution for the inverse function  $g^{-1}(v)$  can be derived from a uniform location distribution and a positively monotonic behaviour of the velocity, i.e.:

$$s = g^{-1}(v) = F_{\underline{v}}(v) (g^{-1}(v_m) - g^{-1}(v_o)) + g^{-1}(v_o) \quad (1)$$

where  $v_m$  and  $v_o$  are the observed or specified velocities at locations in the cross-section  $s_m = g^{-1}(v_m)$  and  $s_o = g^{-1}(v_o)$ , respectively.

In case a non-monotonic behaviour in terms of the location variable is simulated (e.g., in the case of the dip-phenomenon), then we analyse separately each monotonic branch  $\zeta(s)$  for the velocity (or  $\psi(s)$  and  $\omega(s)$ , for the pressure and water-depth, respectively) and derive afterwards the required segments of the profile  $g(s)$  by appropriate formulations (see more details in Dimitriadis et al., 2019b, sect. 3.3).

Table 1: Probability distributions for the sampling location (ME0), longitudinal velocity (ME2 and ME3), pressure (ME1 and ME2), and water-depth (ME1 and ME2) as derived in the companion work of Dimitriadis et al. (2019b). Note that all distributions are illustrated for convenience for the velocity but can be easily applied for the other variables. Also, for convenience, we present either the distribution function  $F_{\underline{v}}(v)$  or its density  $f_{\underline{v}}(v)$ , but one may easily estimate the one from the other through  $F_{\underline{v}}(v) = \int_{-\infty}^v f_{\underline{v}}(x) dx$  and  $f_{\underline{v}}(v) = dF_{\underline{v}}(v)/dv$ .

| Abbreviation | Probability distribution function  |
|--------------|--|
| ME0          | $F_{\underline{v}}(v) = \frac{v - v_o}{v_m - v_o} \quad (2)$   |
|              | where $v_o$ and $v_m$ are the low and high values at boundaries.   |
| ME1          | $f_{\underline{v}}(v) = e^{-\lambda_0 - \lambda_1 v} \quad (3)$  |
| ME2          | $f_{\underline{v}}(v) = \frac{\varphi(v; \mu, \sigma)}{1 + \Phi(v; \mu, \sigma)} \quad (4)$  |
|              | where $f_{\underline{v}}(v)$ is the Gaussian distribution low-truncated at zero, $\mu$ and $\sigma$ are the mean and standard deviation without the truncation, and $\varphi(v; \mu, \sigma) = e^{-((v-\mu)/\sqrt{2\sigma^2})^2} / \sqrt{2\pi\sigma^2}$ and $\Phi(v; \mu, \sigma) = 1/2 + 1/2(\text{erf}((v - \mu)/\sqrt{2\sigma^2}))$ are the density and cumulative Gaussian distribution $N(0,1)$ , respectively (also written as $\Phi(v)$ and $\varphi(v)$ ). |
| ME3          | $f_{\underline{v}}(v) = e^{-(\lambda_0 + \lambda_1 v + \lambda_2 v^2 + \lambda_3 v^3)} \quad (5)$  |
|              | where $\lambda_0, \lambda_1, \lambda_2$ , and $\lambda_3$ are the Lagrangian parameters (similarly for the ME1).   |
| PBF          | $F_{\underline{v}}(v) = 1 - (1 + (v/p_1)^{p_2})^{-p_3} \quad (6)$  |
|              | where $p_1, p_2$ , and $p_3$ are shape and scale parameters.   |

### 3. Applications

In this section we present several applications for the demonstration of the concept and the presented framework.

### 3.1. One-dimensional flow cases

#### 3.1.1. Generalized von Kàrman model for boundary and viscous sublayers

In the companion work of Dimitriadis et al. (2019b; sect. 2.3), we illustrate how the original von-Kàrman 1d velocity profile in a channel with high width-to-depth ratio can be derived using the presented framework by starting from the water surface and by rejecting the solution of the negative first spatial derivative of the velocity, which is hydraulically non-feasible in typical cases. We also show how, in general,  $2^{n_v}$  parts of a profile can emerge from all the possible combinations when dividing the first derivative in  $n_v$  monotonic branches. However, the break of the first derivative from a positive to a negative value, and vice versa, occurs when a zero value of the velocity derivative with respect to depth is reached, so that the shear stress model is smoothly transformed from the one condition to the other. This smooth transformation takes place at the mode (most probable) value of the velocity distribution, where the derivative of the distribution also changes sign. Additional distributions must be applied for additional breaks. For example, if we wish to combine two breaks (i.e., three parts), one in the profile area of high depths to characterize the viscous sublayer (i.e., from  $d - b$  depth measured from the water surface to  $d$ , where  $d$  is the maximum water-depth at the cross-section), and one in the profile area of low depths (i.e., near the water surface from 0 to  $d - b$ ) to characterize the dip-phenomenon, then the velocity distribution should be comprised of two part. Since both areas are rarely of practical interest in the same flow case, here we show one application for each case (for the dip-phenomenon see next section). Inside the viscous sublayer (roughness area), the most typical velocity profile is that of Couette flow (i.e., linear velocity profile over the depth due to constant shear stress) that can be derived by employing the ME0 distribution for the high-depth area between depths  $d - b$  and  $d$ . For the remaining area, down to zero-depth, the reformulated von Kàrman profile is employed, with the velocity set to zero at the maximum depth  $d$ , i.e.  $g(y) = \alpha \ln(d/b - y/b + 1)$ . The latter profile can be derived in a similar manner as in Dimitriadis et al. (2019b, sect. 2.3) from a truncated ME1 distribution between  $v_m$  and  $v_b$  of  $\zeta(y) = 2v_m - g(y)$ , where  $v_m = \alpha \ln(d/b + 1)$  and  $v_b = 2v_m - g(d - b) = 2\alpha \ln(d/(b\sqrt{2}) + 1/\sqrt{2})$ .

Therefore, the velocity distribution for the mixed profile can be written as (Fig. 1):

$$f_{\underline{v}}(v) = \begin{cases} \frac{(d+b)^2 e^{-v/\alpha}}{ab(d-b)} C, & v_m \leq \zeta(y) \leq v_b \\ \frac{1-C}{a \ln(2)}, & v_b < \zeta(y) \leq 2v_m \end{cases} \quad (7)$$

with  $C = (d - b)/d \leq 1$ , so that the integral of the above distribution equals 1.

For the uniform distribution of the location variable, i.e.  $f_{\underline{y}}(y) = 1/d$ , the velocity profile can be expressed as (Fig. 1):

$$v/\alpha = \begin{cases} \ln(d/b - y/b + 1), & 0 \leq y \leq d - b \\ \frac{\ln(2)}{b}(d - y), & d - b \leq y \leq d \end{cases} \quad (8)$$

Note that although the profiles and distributions for the location and velocity are continuous at  $v_b$ , the velocity distribution density is discontinuous due to the change of the distribution type.

The above profile has two parameters, the scale-parameter  $a$  and the shape-parameter  $b$ , similarly to the Chiu (1987;1988;1989) generalized von Kàrman profile for 1d flow in open-channel with large depth-to-width ratio. It can additionally preserve the laminar flow conditions in the viscous sublayer within a single expression, which however requires two branches, due to the twofold flow condition. In case the viscous sublayer is of small (or no) interest, one may employ only the first branch of the above expression, or equivalently, use Chiu's original generalized model. Since the viscous sublayer thickness is linked to the roughness coefficient, it would be interesting to test whether this profile can also simulate the effect from channel roughness (Chiu, 1991; Greco et al., 2014; Singh, 2014; Greco, 2015; Greco and Mirauda, 2015; Greco and Moramarco, 2015; Wibowo, 2015). It is noted that this framework can be also applied through alternate entropy measures such as the Tsallis entropy (Sing and Luo, 2011; Cui and Singh, 2013; 2014; Kumbhakar et al., 2019b,c; cf. Dingman, 1989) and Renyi entropy (Kumbhakar and Ghoshal, 2016; Khozani and Bonakdari, 2018).

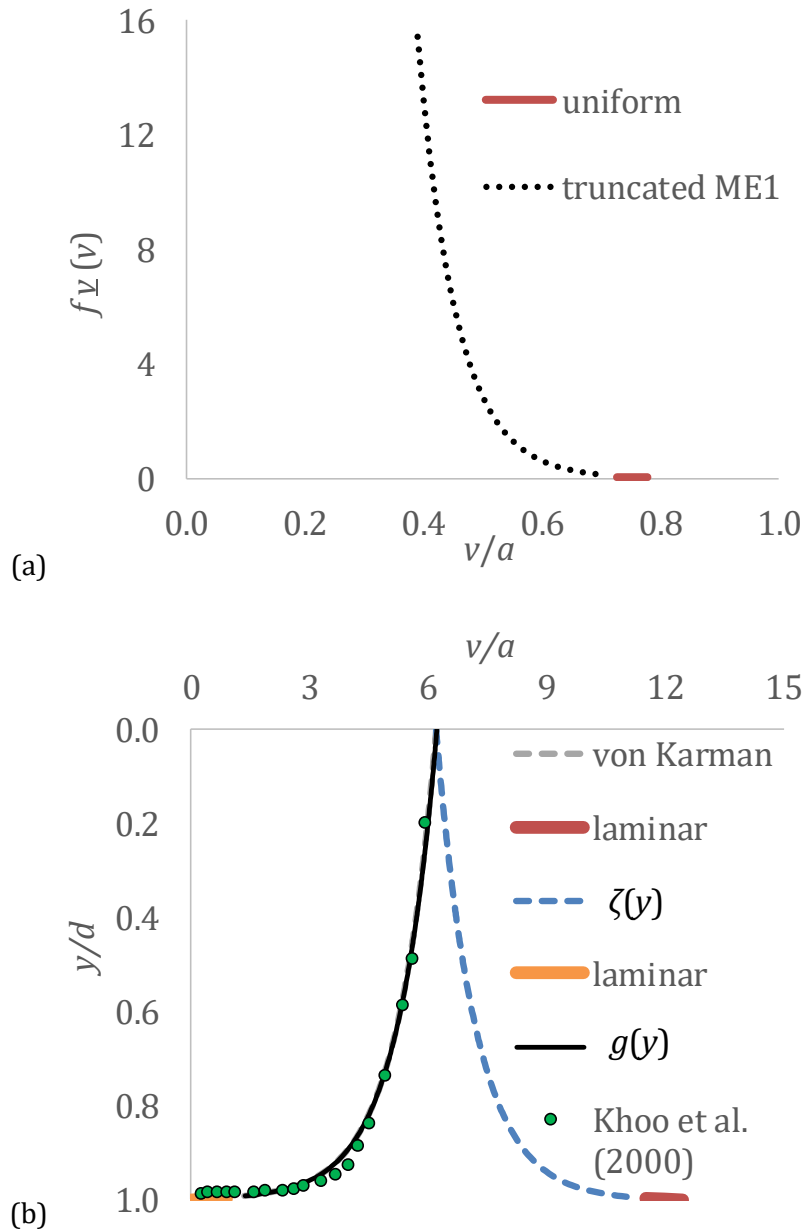


Figure 1: (a) The velocity distribution density function for the mixed truncated ME1 and uniform ME0 and (b) the velocity profiles measured at the boundary and sub-viscous layers for an open-channel flow (data extracted graphically from Khoo et al., 2000, Fig. 1, with Reynolds number 4100, and for a von Kàrman constant 0.4), for the best-fit original and mixed case of the von Kàrman model (with parameters  $\alpha = 0.067$  m/s,  $b = 0.002$  m and  $d = 1$  m), and the Couette linear model (corresponding to laminar flow conditions).

### 3.1.2. The velocity profile with dip-phenomenon in an open-channel flow

The so-called dip-phenomenon corresponds to open-channel flow conditions where the maximum velocity occurs below the water surface, and is often attributed to the boundary and shear stress effects from the side banks of the channel and the water surface (Yang et al., 2004;

2012; Gou and Julien, 2005). Chiu (1987) shows how to express this profile in 1d configuration by conserving only the first moment constraint (i.e. mean) and by introducing two additional parameters, one for the magnitude of the maximum velocity and one for its location along the vertical. This model has been then expanded to 2d configuration to express the spatial structure of the dip-phenomenon in the cross-section (Chiu, 1988; Xia, 1997; Chen and Chiu, 2004; Moramarco et al., 2004; Chiu et al., 2005; Papadimitrakakis and Orphanos, 2009; Chiu and Hsu, 2006; Moramarco et al., 2017). Here, we attempt to implicitly simulate this phenomenon by conserving additionally the second and third raw moments as also performed by Chiu, (1989), Barbe et al. (1991) and Kumbhakar et al. (2019a, and references therein), but without the need to explicitly introduce the parameters of the location and magnitude of the maximum velocity.

Following the same analysis as in the previous section, we can represent the dip-phenomenon with an ME2 velocity distribution truncated at the surface velocity  $v_s$  and at the bottom velocity  $2v_m$ , so that the velocity at the location of the dip at depth  $h$  is  $v_m$  (for this technique, see the companion work of Dimitriadis et al., 2019b, sect. 3.3):

$$f_{\underline{v}}(v) = \frac{\varphi(v; \mu, \sigma)}{\Phi\left(\frac{2v_m - \mu}{\sigma}; \mu, \sigma\right) - \Phi\left(\frac{v_s - \mu}{\sigma}; \mu, \sigma\right)} \quad (9)$$

where  $\mu = v_m$  and  $\sigma$  are the model parameters, and  $v_s$  the surface velocity.

Then, the resulting velocity profile for uniform sampling would be:

$$\left| \frac{d\zeta(y)}{dy} \right| = \frac{\sigma^2 \sqrt{2\pi} \left( \Phi\left(\frac{2v_m - \mu}{\sigma}; \mu, \sigma\right) - \Phi\left(\frac{v_s - \mu}{\sigma}; \mu, \sigma\right) \right)}{d e^{-\frac{(\zeta(y) - \mu)^2}{2\sigma^2}}} \quad (10)$$

which has the positively monotonic solution with respect to depth

$$\zeta(y) = \sigma \sqrt{2} \operatorname{erfinv} \left( \frac{y}{d} \operatorname{erf} \left( \frac{v_s - \mu}{\sigma \sqrt{2}} \right) \right) + \mu \quad (11)$$

where erf is the error function (see more details in Dimitriadis et al., 2019b, sect. 3.3) and erfinv its inverse function (for approximations on both see e.g., Winitzki, 2008).

If we again adopt the reasonable assumption that the shear stress decreases from the channel bottom to the location of the dip and then increases up to the water surface, the velocity profile can be finally written as:

$$g(y) = \begin{cases} \zeta(y), & v_s \leq \zeta(y) \leq v_m \text{ and } 0 \leq y \leq h \\ 2v_m - \zeta(y), & v_m \leq \zeta(y) \leq 2v_m \text{ and } h \leq y \leq d \end{cases} \quad (12)$$

A more accurate distribution for the dip phenomenon would be the ME3. Here, instead of

employing directly the ME3 distribution, we fit the PBF with the method of moments, which moments are more easily handled than those of the ME3, and at the end we fit the ME3 to the PBF with the simple least-square method (for a direct simulation of the ME3 see Kumbhakar et al., 2019a). Once the limits are known (i.e. physically justified and/or observed), the PBF distribution is low-truncated at the surface velocity  $v_s$  and high-truncated at  $2v_m$ , where  $v_m$  is the maximum velocity occurring at depth  $h$ , since we again assume zero velocities at boundaries (i.e. no slip-condition). So, for the velocity we have that:

$$F_{\underline{v}}(v) = \frac{(1 + (v_s/p_1)^{p_2})^{-p_3} - (1 + (v/p_1)^{p_2})^{-p_3}}{(1 + (v_s/p_1)^{p_2})^{-p_3} - (1 + (2v_m/p_1)^{p_2})^{-p_3}} \quad (13)$$

From Eqn. 1, we can derive the function  $\zeta(y)$  as:

$$\zeta(y) = p_1 \left( \left( \left( 1 + \left( \frac{v_s}{p_1} \right)^{p_2} \right)^{-p_3} - \frac{y}{d} \left( \left( 1 + \left( \frac{v_s}{p_1} \right)^{p_2} \right)^{-p_3} - \left( 1 + \left( \frac{2v_m}{p_1} \right)^{p_2} \right)^{-p_3} \right) \right)^{-1/p_3} - 1 \right)^{1/p_2} \quad (14)$$

We again initially select the positive solution of the above profile, since we assume the velocity to increase with respect to depth, and after the velocity reaches a maximum value  $v_m$  (i.e. zero spatial derivative at depth  $h$  of each vertical) we select the negative solution, since we assume that the shear stress changes sign after reaching its maximum (Fig. 2).

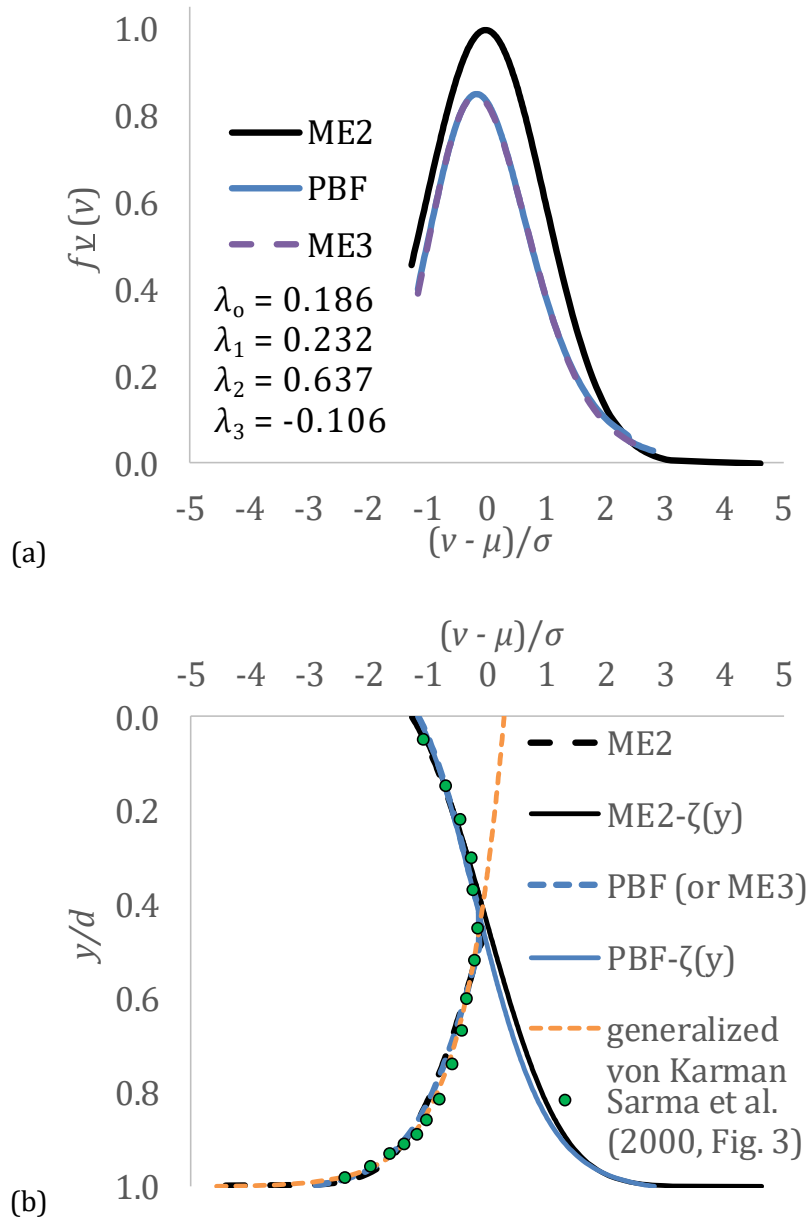


Figure 2: (a) The velocity distribution density function for the truncated ME2, PBF and ME3, and (b) the velocity profiles for the dip-phenomenon in a smooth rectangular open-channel (data extracted graphically from Sarma et al., 2000, Fig. 3, with width-to-depth ratio approximately 5, Froude number 1.6, shear velocity 0.124 m/s), for the best-fit truncated ME2 distribution (Nash–Sutcliffe efficiency coefficient 0.971) with parameters  $v_s = 1.35$  m/s,  $v_m = \mu = 1.85$  m/s and  $\sigma = 0.4$  m/s ( $h$  is estimated from the model as 0.45 m), the truncated PBF distribution at  $v_s = 1.35$  m/s (Nash–Sutcliffe efficiency coefficient 0.977) with parameters  $p_1 = 2.298$ ,  $p_2 = 5.162$  and  $p_3 = 1.785$  (so that the mode velocity is again  $v_m = 1.85$  m/s), the ME3 distribution with parameters shown in the upper panel, and the best-fit generalized von Kàrman model as derived above, i.e.  $g(y) = \alpha \ln(d/b - y/b + 1)$ , with parameters  $\alpha = 0.28$  m/s and  $b = 0.0009$  m.

Interestingly, in the case of the dip-phenomenon, the model proposed by Chiu (1988) introduces an extra parameter  $h$  for the location of the maximum velocity, whereas the above model requires the surface velocity (which, for consistency, is considered as constraint only after it is observed),

from where the location of the dip can then be estimated from the magnitude of the difference between  $v_m$  and  $v_s$ , which is mapped onto the difference between the two locations of the maximum and surface velocity. In other words, both approaches require three parameters, but the proposed one is more flexible since it depends entirely on the selection of the probability distribution, uses the extra parameter for the simulation of variance (and skewness if the ME3 or PBF is applied) and can simulate the Boussinesq and Coriolis parameter (if needed); and may be more consistent with the observations and improve fitting. We also see that quite satisfactory results are obtained if the ME2 solution is adopted and for the examined case we suggest that there is no need for an additional parameter only to slightly improve the fitting. Interestingly, as shown by Dimitriadis et al. (2019), various cases of open-channel flows in natural cross-sections result in nearly-Gaussian empirical distributions of the longitudinal velocity.

### 3.1.3. One-dimensional pressure profiles at a stepped spillway

As discussed in Dimitriadis et al. (2019b, sect. 3), the pressure variable is linked to the water-depth variable and when their distributions have the same shape and only differ in their expected value, then the pressure profile is hydrostatic. Although in open-channel flows the latter profile is often assumed, there are many cases where the pressure is non-hydrostatic (Castro and Hager, 2017), as for example in standing waves (e.g. Yuan, and Wu, 2004), in hydraulic jumps (e.g. Hervouet, 2003), in aquifers near hydraulically connected streams (e.g. Koussis et al., 2007), in rapidly varied flows (e.g. Zerihun, 2017), in flow over weirs (e.g. Naghavi et al., 2011; Felder and Chanson, 2012), ramps (Mohamed, 2004) etc. In this application we examine the pressure profiles in stepped spillways, where an over-hydrostatic pressure occurs upstream of the step due to the curved streamlines and an under-hydrostatic pressure occurs downstream of the step due to cavity and the streamlines separation (Zhang and Chanson, 2016). We fit an ME1 distribution to the pressure profile truncated at the observed pressure at the bottom of the spillway at depth  $d$ . Similarly to the von Kàrman velocity profile, but with the pressure increasing with depth, the pressure profile can be written as (Fig. 3):

$$p/P = \alpha \ln \left( \frac{1}{1 - y/d \left( 1 - e^{-\frac{p_m}{\alpha P}} \right)} \right) \quad (15)$$

where  $p_m$  is the maximum pressure at the maximum depth (i.e. bottom of the spillway),  $P = \gamma d \cos \varphi$  the hydrostatic pressure,  $d$  the water depth, and  $\cos \varphi$  the local topographic slope at the spillway.

For the above profile see also the work of Barbe et al. (1994), where a pressure profile is derived for groundwater flow based on the conservation of mass. We again comment that the above model contains one parameter (ME1) plus the pressure at bottom, which, for consistency, is considered as constraint only after it is observed. In other words, the profile is still valid for an infinite pressure magnitude at infinite depth  $d$ , and in particular, it corresponds to the original exponential probability distribution, without high-value truncation. After we observe both depth  $d$  and pressure at bottom  $p_m$ , we may add these as constraints and employ the above expression.

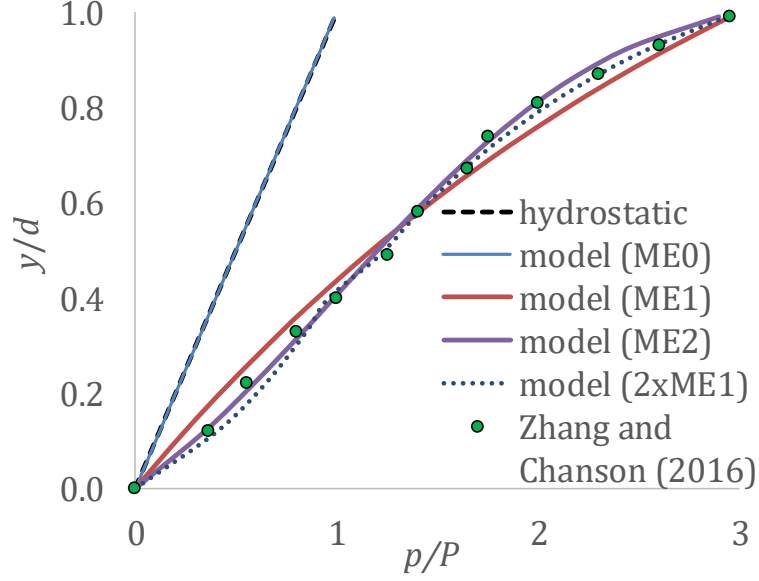


Figure 3: The pressure profile upstream of a step in a stepped-spillway (data extracted graphically from Zhang and Chanson, 2016, Fig. 5A), the best-fit profile resulted from the truncated ME1 distribution with parameters  $a = 3.33$ ,  $p_m/P = 3$ , the best fitted profile from two truncated ME1 as derived below (see Eq. 16) with parameters  $\alpha_s = 0.9$  and  $b = 0.2$  m (also, for illustration, it is shown the best-fit profile from the truncated ME2 as derived in the previous section, with parameters  $\mu = 1$ ,  $\sigma = 1.1$ ,  $p_m/P = 3$ ; see discussion for the ME2 when  $C_v > 1$  in Dimitriadis et al., 2019b, sect. 3.3), and the theoretical and modelled hydrostatic profiles.

For the pressure downstream of the step, the profile changes due to cavity with the maximum pressure occurring above the channel bottom, resembling the dip-phenomenon for the velocity described in the previous section. In particular, the profile along the vertical now comprises two parts, a similar to the previously studied one and another one starting at the bottom of the spillway. The pressure profile can be derived in a similar manner as in sect. 3.1.1, but now from two separate ME1. The first one truncated at  $p_m/P$  and  $(2p_m - p_b)/P$ , where  $p_b/P$  is the pressure at the channel bottom due to cavity, and the other one truncated at  $p_m/P$  and  $2p_m/P$ , where  $p_m/P = \alpha \ln(d/b + 1)$ , both corresponding to the monotonically positive function  $\psi(y)$ , with  $\psi(y) = 2p_m - g(y)$  for  $0 \leq y \leq h$  and  $\psi(y) = g(y)$  for  $h \leq y \leq d$ , where  $h$  is the depth of the meeting point of the two parts. Thus, for the uniform distribution of the location variable, i.e.  $f_y(y) = 1/d$ , the pressure profile can be expressed as (Fig. 4):

$$p/P = \begin{cases} \alpha_s \ln(y/b + 1), & 0 \leq y \leq h \\ \alpha_b \ln(d/b - y/b + 1) + p_b/P, & h \leq y \leq d \end{cases} \quad (16)$$

where  $\alpha_s$  is a parameter,  $\alpha_b = (\alpha_s \ln(h/b + 1) - p_b)/\ln(d/b - h/b + 1)$ . The pressure parameter, i.e.  $\lambda = E[p/P]$  (Yen, 1973; Dimitriadis et al., 2019b), for the above profile can be estimated as 0.87 (for the part of the profile close to the water surface as 0.81 and for the upper-part as 1.02), indicating the well-known result that cavity causes an overall sub-hydrostatic effect.

We note that although the profiles and distributions for the location and pressure are continuous

at  $p_m$ , the distribution density of pressure is discontinuous due to the change of the distribution type. We also comment on the fact that the ME2 model does not fit well the observations and that two different ME1 parts of the profile are required to fit the pressure (also, employing two ME2 is expected to result in a better fitting). We justify the use of two parts for the profile (instead of one as previously shown), since the examined phenomenon contains two different air-water surfaces, each one being close to a hydrostatic behaviour, in the sense that the pressure increases or decreases almost linearly.

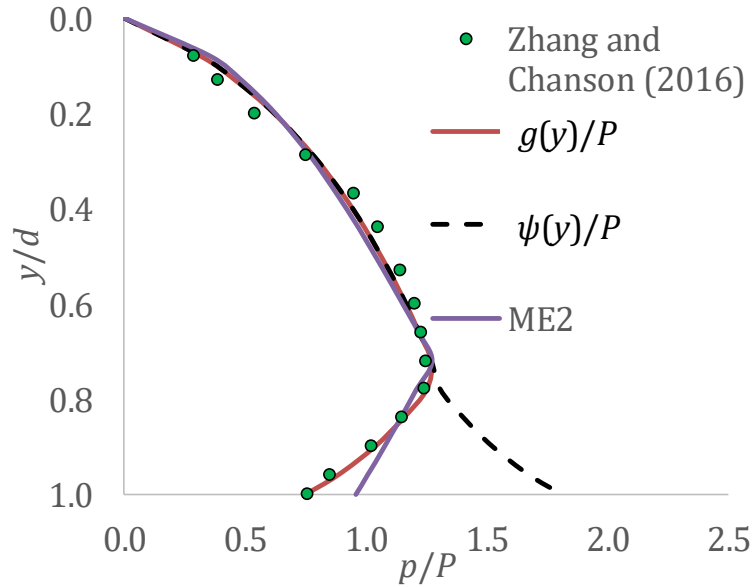


Figure 4: The pressure profile downstream of a step in a stepped-spillway (data extracted graphically from Zhang and Chanson, 2016, Fig. 5E), the best-fit profile resulted from the two truncated ME1 distributions with parameters  $\alpha_s = 0.7$ ,  $b = 0.14$  m, and  $p_b/P = 0.75$  (also observe that  $h/d = 0.75$  and  $\alpha_b = 0.5$ ), and for illustration, it is shown the best-fit profile from the truncated ME2 as derived in the previous section, with parameters  $\mu' = 1.688$ ,  $\sigma' = 0.781$ , and  $p_b/P = 0.75$ .

### 3.2. Axisymmetric pipe-flow profiles

In axisymmetric flows, as in nearly all pipe flows in symmetrical conduit geometries with respect to the pipe centre, the skewness coefficient is zero, i.e.  $C_s = 0$  and  $\alpha = 3\beta - 2$ , where  $\beta$  is the Boussinesq parameter and  $a$  the Coriolis parameter (for non-symmetric geometries in pipe flows see a similar analysis for open-channel flows of irregular geometries in the next section). Therefore, the velocity distribution that maximizes entropy based on the three typical constraints is close to ME2. For the simulation of flow in a pipe of circular cross-section with radius  $R$  (similar analysis can be made for another symmetric geometry such as a square duct), and under maximum pressure  $p_m$  at the bottom of the pipe and minimum pressure  $p_o = p_m - 2R$  at the soffit, we set the origin of the axis again at the soffit of each vertical, and we express the velocity and pressure profiles for each vertical (a similar analysis can be followed in the horizontal direction), with total depth  $d(x) = 2\sqrt{R^2 - x^2}$ , where  $x$  ranges from  $-R$  to  $R$ , and  $y(x) = \sqrt{r^2 - x^2} = x \tan(\theta)$  ranges from 0 to  $d(x)$ , where  $r$  and  $\theta$  are the polar coordinates, i.e. the radius

and anticlockwise angle (Fig. 5). We implement the ME0 distribution for the location of each vertical, with  $y_o(x) = R - d(x)/2$  and  $y_m(x) = R + d(x)/2$ .

For the velocity profile, we employ the ME2 with zero velocities at all boundaries (no-slip condition), i.e., Gaussian distribution with lower-truncation at zero, mean value  $\mu(x) = v_m(x)$  and higher-truncation at  $2v_m(x)$ . This choice is based on the symmetry of the geometry with respect to a parallel to  $y$ - $y$  axis passing through the pipe center, which leads us to expect that the maximum velocity will be at the center of each vertical with equal distance from its boundaries. So, for the velocity we have that:

$$F_{\underline{v}}(v(x)) = \frac{\Phi(v(x)) - \Phi(0)}{\Phi(2v_m(x)) - \Phi(0)} = \frac{1}{2} + \frac{\operatorname{erf}((v(x) - v_m(x))/\sqrt{2\sigma^2(x)})}{2\operatorname{erf}(v_m(x)/\sqrt{2\sigma^2(x)})} \quad (17)$$

where  $\sigma(x)$  is the standard deviation of the non-truncated Gaussian function.

From Eq. 1 (see also the companion work of Dimitriadis et al., 2019b, sect. 2.2), we can derive the function  $\zeta(x, y)$  as:

$$\zeta(x, y) = v_m(x) + \sqrt{2}\sigma(x)\operatorname{erfinv}\left(\left(\frac{y(x)}{\sqrt{R^2 - x^2}} - 1\right)\operatorname{erf}\left(\frac{v_m(x)}{\sqrt{2}\sigma'(x)}\right)\right) \quad (18)$$

where  $\operatorname{erfinv}(x)$  is the inverse of the error function.

We initially select the positive solution of the above profile, since we assume the velocity to increase with respect to the depth, and after the velocity reaches a maximum value (i.e. zero spatial derivative at the half-depth for each vertical) we select the negative solution, since we assume that the shear stress changes sign after reaching its maximum (Fig. 5). So, the velocity profile is:

$$g(x, y) = \begin{cases} \zeta(x, y), & 0 \leq y(x) \leq d(x)/2 \\ 2v_m(x) - \zeta(x, y), & d(x)/2 \leq y(x) \leq d(x) \end{cases} \quad (19)$$

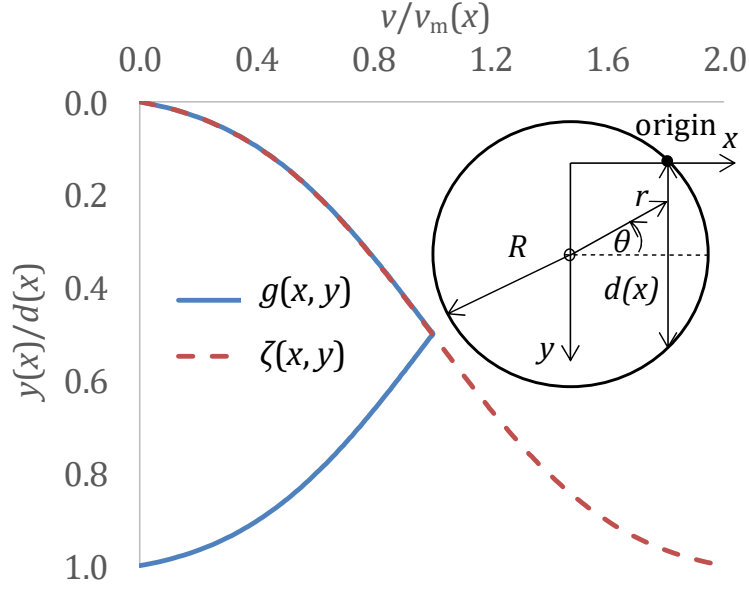


Figure 5: An example of the derived velocity profile  $g(x, y)$  and the monotonic profile  $\zeta(x, y)$  for  $\mu(x) = v_m(x) = 2$  and  $\sigma(x) = 1$ .

In terms of pressure, if a hydrostatic profile is assumed, then the probability distribution will be similar to that of the depth, since the two variables are linearly connected through  $p = \psi(r, \theta) = p_o + R - r\sin(\theta)$ , with  $\bar{p} = p_o + R$ . The absolute derivative of the inverse pressure profile is  $|\mathrm{d}\psi^{-1}(p(x))/\mathrm{d}p(x)| = (p_m(x) - p_o(x))/d(x) = 1$ , which results in  $y(x) = \psi^{-1}(p(x)) = \pm (p(x) - p_o(x))$ . By adopting the positive solution for each vertical (since we have assumed the pressure to increase with depth), we have that  $\psi(x, y) = p_o(x) + y(x)$ , with  $p_o(x) = p_o + R - d(x)/2$  and  $p_m(x) = p_o(x) + d(x)$ . The isobaric lines are then parallel to the  $x$ - $x$  axis, i.e. independent of the position  $x$  in the cross-section, whereas the isovels are circles, i.e. they only depend on the radius  $r$ . Also, in the case of a hydrostatic profile, the pressure model requires a single pressure observation in the cross-section, e.g. at the centre  $p_c$ , so that the minimum pressure at the pipe soffit can be calculated as  $p_o = p_c - R$  and thus,  $\psi(r, \theta) = p_c - r\sin(\theta)$ .

We observe that  $g(x, y)$  is symmetric to a parallel to the  $x$ - $x$  axis passing from the pipe centre. Thus, for convenience, we may change the Cartesian location variables  $x$  and  $y$  to the polar ones by  $x = r\cos(\theta)$  and  $y = r\sin(\theta)$ , with the radius  $r$  ranging from  $r_o = 0$  to  $r_m = R$ , and the angle  $\theta$  ranging from  $\theta_o = 0$  to  $\theta_m = 2\pi$ , both following the ME0 distribution. The isovels  $g(x, y)$  are now circles around the center of the pipe and independent of the angle  $\theta$ , and we may write  $g(r)$ . Thus,  $F_r(\zeta'^{-1}(v(r))) = (\zeta'^{-1}(v(r)) - \zeta'^{-1}(v(R)))/(\zeta'^{-1}(v(0)) - \zeta'^{-1}(v(R))) = \pi r^2/(\pi R^2) = (r/R)^2$ , and  $f_r(\zeta'^{-1}(v(r))) = 2r/R^2$ , where  $\zeta'$  is the positively monotonic function for the velocity with respect to the radius measured from the pipe center. Finally, the velocity profile can be expressed with the parameters  $\mu = v_m$  and  $\sigma$  now assumed fixed for the whole cross-section, i.e.:

$$v = g(r) = v_m - \sigma\sqrt{2}\operatorname{erf}\operatorname{inv}\left(\left(\frac{r}{R}\right)^2 \operatorname{erf}\left(\frac{v_m}{\sigma\sqrt{2}}\right)\right) \quad (20)$$

For the estimation of the two parameters of the above velocity model, two measurements are needed for each vertical in the cross-section. A careful look at the derived profile for the overall section and for each vertical, reveals that the standardized velocity profile by  $v_m$  and  $v_m(x)$ , depends only on the variability coefficient, and in fact,  $C_v = \sigma/v_m = \sigma(x)/v_m(x)$ . Therefore, if we sample the velocity at the pipe centre, and we assume a fixed variability  $C_v$ , we can determine the streamflow just by the mean velocity. Although an analytical solution for the mean velocity is not possible, we derive a fair approximation (numerical solution may result in higher accuracy):

$$\bar{v} \approx v_m + \frac{\sigma\sqrt{2} \left( e^{-\operatorname{erf}^{-1}\left(\operatorname{erf}\left(\frac{v_m}{\sigma\sqrt{2}}\right)\right)} - 1 \right)}{\sqrt{\pi} \operatorname{erf}\left(\frac{v_m}{\sigma\sqrt{2}}\right)} \quad (21)$$

We further observe that the parameter  $\sigma$  controls the flow conditions in a variety of cases. For example, consider the semi-empirical expression  $v(r) = v_m(1 - r/R)^{1/7}$  (else known as 1/7 profile; e.g. Bogue and Metzner, 1963) for turbulent pipe flow conditions (Reynolds number  $Re = \bar{v}D/\nu > 4000$ ;  $D$  is the pipe diameter,  $\bar{v}$  the mean velocity, and  $\nu$  the kinematic viscosity  $\approx 10^{-6} \text{ m}^2/\text{s}$  for water at 20°C). We can approximate this profile by the proposed model for  $\sigma/v_m \approx 0.23$  (Fig. 6), giving the Boussinesq and Coriolis parameters  $\beta = 1.05$  and  $\alpha = 1.16$  (see definitions in the companion work of Dimitriadis et al., 2019b, sect. 3.2).

Moreover, Fig. 6 shows that in case the mean velocity tends to very small values ( $Re \ll 4000$ ), we get an excellent match of the theoretically derived laminar profile for pipe flows  $v(r) = v_m(1 - (r/R)^2)$  if we assume a uniform velocity probability distribution (i.e. no constraints). However, such conditions are rare in natural flows, where the mean velocities are much higher than zero, the physical dimensions large and intense mixing occurs among streamlines. Finally, note that in a purely deterministic analysis, the turbulent model is far more complicated to derive than the laminar one, whereas in a probabilistic-deterministic framework one may derive both relatively easily; this is a strong advantage of the latter for the analysis of natural flows.

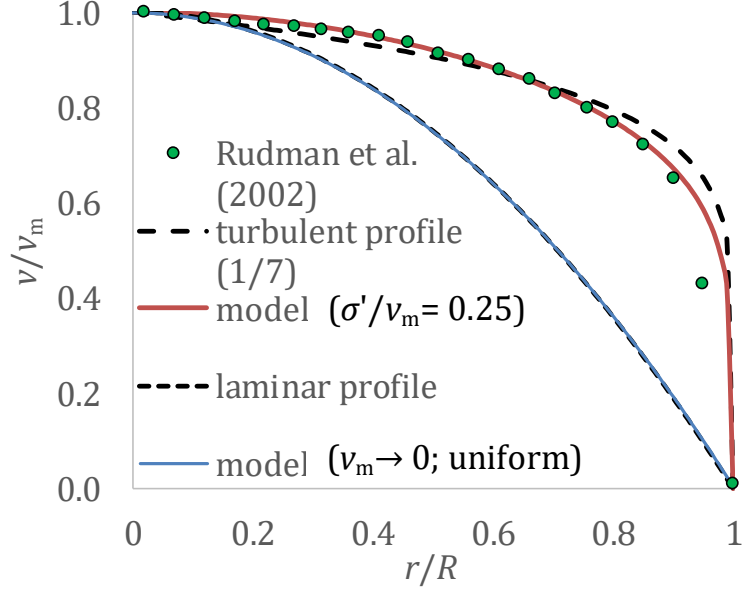


Figure 6: Velocity profiles for a smooth turbulent pipe flow (data extracted graphically from Rudman et al., 2002, Fig. 7, which includes experimental measurements and direct-numerical-simulations at a pipe flow with Reynolds number approximately 5000), for the best-fit model ( $\sigma'/v_m = 0.25$ ), for the semi-empirical velocity 1/7 profile for turbulent flow conditions, and for the theoretically derived and modelled ( $\sigma'/v_m \rightarrow \infty$ ) profile for laminar flow conditions.

The proposed model for the velocity profile contains two parameters since it is explicitly defined through the velocity probability distribution (i.e. two-parameter ME2). For circular pipe flow the commonly applied models are derived by conserving one moment (i.e. one-parameter ME1), and by introducing an additional parameter for the maximum velocity at the center of the pipe (Chiu et al., 1993; Chiu and Hsu, 2006; Yoon et al., 2012; Jiang et al., 2016; Choo et al., 2017; Kazemian et al., 2018). Besides the difference in configuration between that model and the proposed one, a theoretical and practical merit of the latter ME2 model is its greater flexibility in conserving the momentum (Boussinesq) parameter, while the former assumes a momentum parameter derived from the variance of the truncated exponential distribution. Similarly, the kinetic energy (Coriolis) parameter for both approaches cannot be set arbitrarily; it depends exclusively on the values of the two model-parameters, from which skewness can be easily calculated. One could employ the ME3 distribution for the pipe flow and include the effect of skewness as an extra parameter, but only for non-axisymmetric geometries.

### 3.3. Two-dimensional open-channel profiles

In this section, we present two applications in two-dimensional (2d) velocity profile and in the distribution of water depth. The ME1 is usually applied for the variability of the water-depth along the water surface of a natural cross-section, as in the design of irrigation ditches (Greco, 2016), for bathymetry estimation (Moramarco et al., 2013; 2019; Farina et al., 2015), at the structure of furrow geometry (Sighn, 2012), and in open-channel with submerged aquatic plants (Chen and Kao, 2011). Here, we express the water-depth at each point of the cross-section again as a random variable. This definition may be considered plausible since the water-depth at a water point in the section is trivially estimated as its distance from the water surface. However, this definition is consistent with the definition of the velocity and pressure in the sense that all three are considered

as variables of a water lump in a cross-section. In this way, the same framework can be easily applied to water-depth and other variables can be also added (such as temperature, salinity etc.) along with the appropriate hydraulic conservation equations.

The isolines of location can be formulated by radially estimating the equal specific distances from the boundaries of the cross-section to the origin point, which is defined as the point influenced the least by the boundaries. By assuming that the same friction applies to all channel boundaries (sides and bottom), the origin point is set at the middle of the water surface in the case that no dip-phenomenon occurs, or, otherwise, at a lower from the surface point in the scenario that the friction at the air-water surface (in case of low velocities at surface) and effects from the surrounding boundaries (in case of low width-to-depth ratios) can no longer be assumed negligible. For example, in the case of a trapezoidal cross-section of maximum depth  $d$ , upper-width  $w_u$  and lower-width  $w_l$  (Fig. 7), we may approximate the ratio of the area of the cross-section with height  $y$  over the total area of the cross-section as (similarly to the sampling location distribution of the circular pipe as derived in sect. 3.2):

$$F_y(\omega^{-1}(y)) \approx \frac{w_u + w_l - 4(d - y)}{w_u + w_l} y/d \quad (22)$$

which for high width-to-depth ratios results in  $F_y(y) \approx y/d$ . So, the isoline of a location with height  $y$  of the vertical passing from the origin point can be easily drawn by locating all points  $(y, \theta)$  with the same specific distance  $y/d$  as measured by the ratio of their distance from the origin point to the distance along a line with angle  $\theta$  from the origin point to the channel boundary.

After we express the distribution for the location variable, we may derive the water-depth profile by employing the ME1 distribution rather than the ME2. So, the water-depth profile along a line with specific distance  $y/d$  (measured along the vertical line passing from the origin as explained above), can be written as:

$$w/d = \ln\left(\frac{1}{1 - y/d(1 - e^{-w_m/d})}\right) \quad (23)$$

where  $w_m = d$  is the maximum water-depth in the trapezoidal cross-section.

Note that the ME2 has been also applied but with minor improvement in fitting (Fig. 7) compared to the adding of an extra parameter to the model.

Concerning the variability of the velocity in a 2d cross-section, we analyze the same dataset. Two-dimensional open-channel models with high width-to-depth ratios have been proposed for the ME1 model for rectangular geometry (Chiu, 1988; Araujo and Chaudhry, 1998; Chiu and Tung, 2022; Maghrebi and Rahimpour, 2005; 2006; Marini et al., 2011; 2017; Singh et al., 2013; Fontana et al., 2013; Rahimpour, 2017; Mirauda et al., 2018), trapezoidal geometry (Sheikh and Bonakdari, 2015), irregular shapes (Chiu and Murray, 1992; Chiu and Said, 1995; Moramarco et al., 2004; Farina et al., 2014). Here, we treat an open-channel flow as in the case of the pipe flow (sect. 3.2), and the origin point is set at the maximum velocity point, which is assumed to be the one

influenced the least by the boundaries. Therefore, the origin point is set either in the middle of the water surface (i.e. zero depth) or, in the case that the dip-phenomenon occurs, at a larger depth. Since we assume that the velocity at points with same specific distance from the boundaries will be the same, we can estimate at each point in the cross-section the distance from the origin point, and apply a similar expression for the velocity profile as in the one-dimensional case (sect. 3.1.2):

$$\zeta(r, \theta) = \mu + \sigma\sqrt{2}\operatorname{erfinv}\left(\frac{y}{d(\theta)}\operatorname{erf}\left(\frac{v_s(\theta) - \mu}{\sigma\sqrt{2}}\right)\right) \quad (24)$$

where  $\mu = v_m$ ,  $d(\theta)$  is the total distance from the origin to the channel sides or bottom, which for a trapezoidal cross-section depends on the anticlockwise angle  $\theta$  between the line connecting the origin to the point-of-interest and water surface (Fig. 7), and  $v_s(\theta)$  is the velocity along the water surface. Again to account for the dip-phenomenon (i.e. maximum velocity at depth  $h$  from surface along the vertical at  $\theta = 90^\circ$ ), we formulate a two-branch profile as  $v = \zeta(r, \theta)$ , when  $0 \leq r \leq h$  and  $v_s \leq \zeta(r, \theta) \leq v_m$ , and  $v = 2v_m - \zeta(r, \theta)$ , when  $h \leq \zeta(r, \theta) \leq d$  and  $v_m \leq v \leq 2v_m$ .

For no dip-phenomenon (i.e. for  $h = 0$  and  $v_s = v_m$ ):

$$v = g(r, \theta) = v_m - \sigma\sqrt{2}\operatorname{erfinv}\left(\frac{y}{d(\theta)}\operatorname{erf}\left(\frac{v_m}{\sigma\sqrt{2}}\right)\right) \quad (25)$$

We note that in contrast to the ME1 model, the velocity profile through the ME2 can no longer be standardized by the maximum velocity, due to the non-linear error function. Although both models include the same number of parameters (i.e.,  $\mu$  and  $\sigma$  for the ME2, and  $M$  and  $v_m$  for the ME1 as proposed by Chiu, 1988), the profile derived with ME2 fits better to the measurements (Fig. 8) with and without accounting for the dip-phenomenon. The Nash–Sutcliffe coefficient is further improved if we account for a small dip of the location of the maximum velocity, which can be also physically justified by the fact that the verticals at the left and right side of the channel are not monotonically increase but exhibit a dip-phenomenon not easily apparent in other recorded verticals (see recorded points in each vertical in Chiu, 1988, Fig. 9).

Moreover, we observe that the ME2 model parameters are estimated as approximately equal to those of the no-dip scenario. Therefore, if the parameters of the ME2 model are estimated, and the Boussinesq and Coriolis parameters can be assumed constant for a range of streamflows, then we may express the 2d longitudinal velocity profile (and also estimate the discharge) by recording only the surface velocities and truncating the ME2 distribution (or ME3 as shown in sect. 3.1.2) at these values. Note that the dip-phenomenon in 2d open-channel flow will be further investigated in a follow-up work, and that for unsteady flow conditions a similar to the ME1 approach (Chen and Chui, 2002; Chen et al., 2012; Bechle and Wu, 2014; Pizarro et al., 2017) can be applied for the ME2.

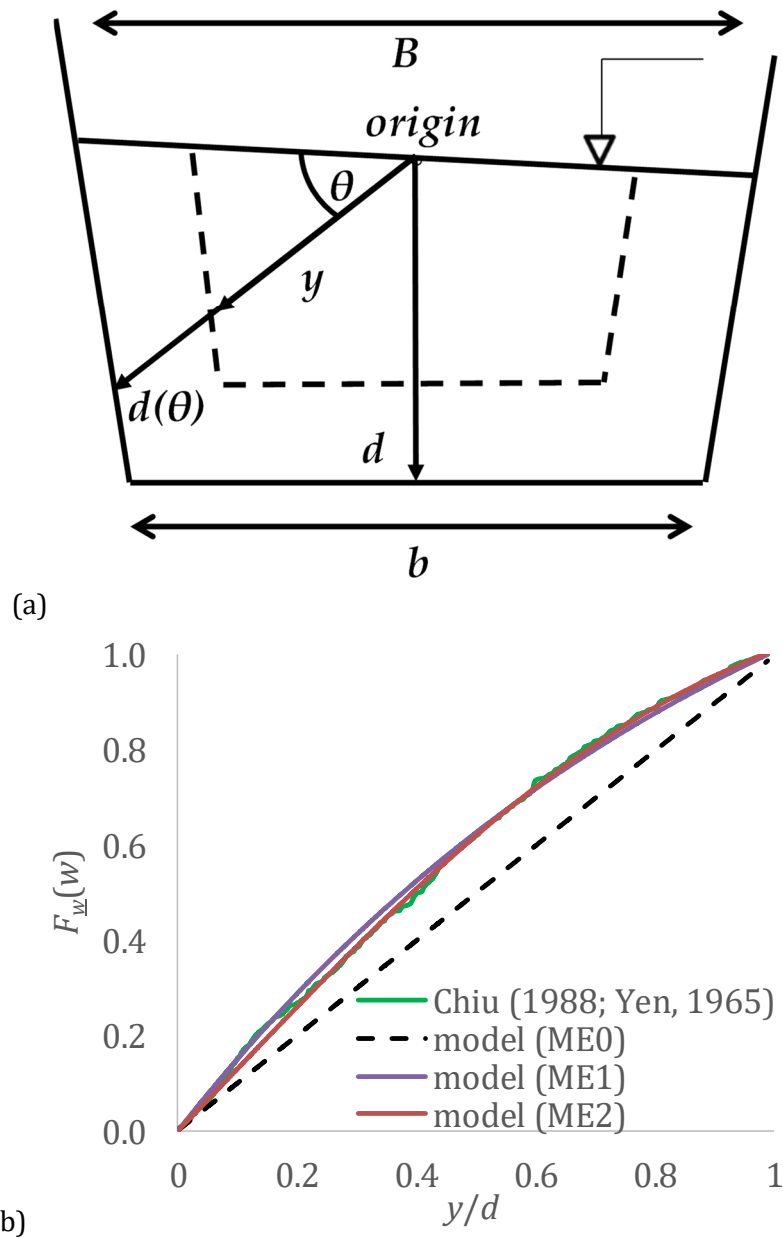


Figure 7: (a) Schematic representation of a trapezoidal cross-section resembling that of Chiu (1988; Fig. 9); and (b) The water depth distribution of a trapezoidal cross-section (data extracted graphically from Chiu, 1988, Fig. 9), the best-fit truncated ME1 distribution (Nash-Sutcliffe coefficient 0.996) with parameters  $a = 1$  and  $w_m/d = 1$ , the best-fit ME2 truncated at 0 and 1 as derived in sect. 3.1.2 (slightly improved 0.999 Nash-Sutcliffe coefficient) with parameters  $\mu = 0.1 < \sigma = 0.6$  (see discussion for the selection between ME1 and ME2 when  $C_v > 1$ , in Dimitriadis et al., 2019b, sect. 3.3), and the theoretical distribution ME0 for a rectangular cross-section.

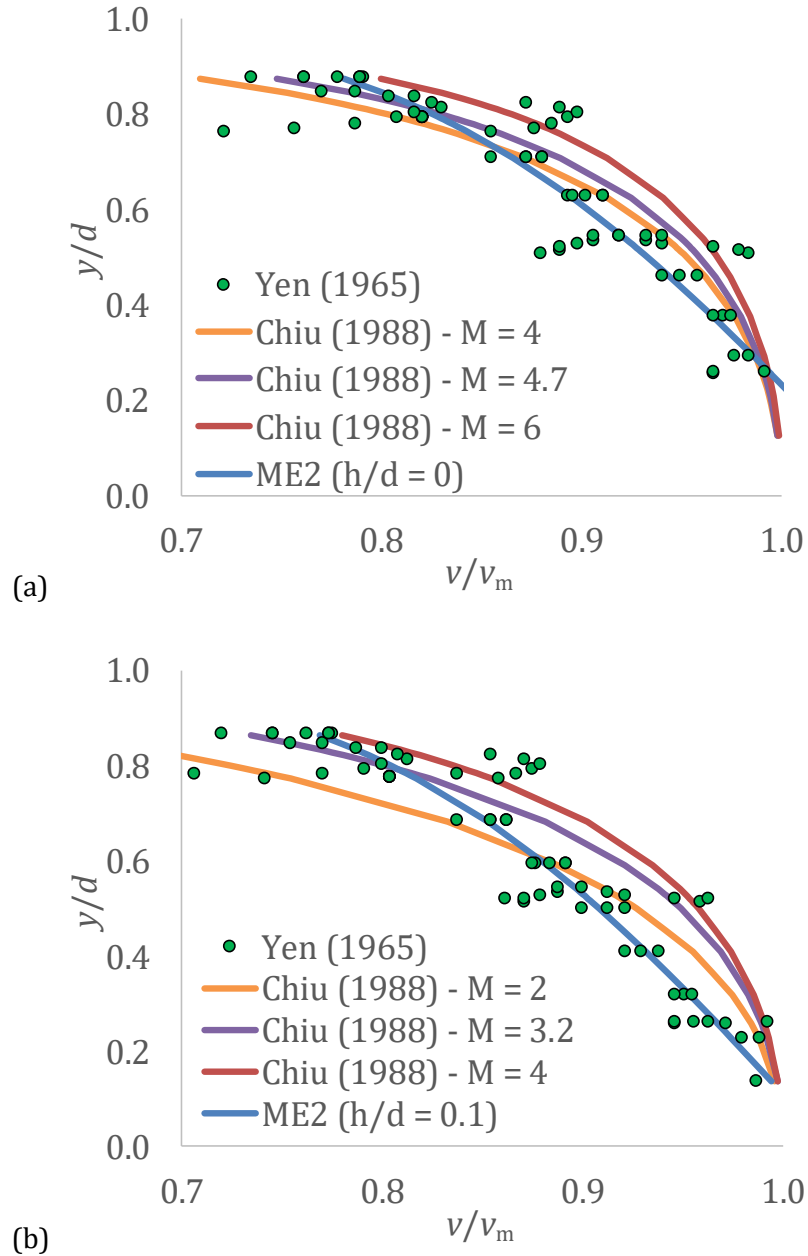


Figure 8: Standardized velocity records from a trapezoidal cross-section (data extracted graphically from Chiu, 1988, Fig. 9), and (a) no simulation of the dip-phenomenon ( $h/d = 0$ ; as also suggested by Chiu, 1988) by the model proposed by Chiu (1988), with parameter  $v_m = 1.14$  m/s and  $M = 4$  (Nash–Sutcliffe coefficient 0.69), optimum  $M = 4.7$  (Nash–Sutcliffe coefficient 0.76) and  $M = 6$  (Nash–Sutcliffe coefficient 0.63), and the ME2 model (truncated at  $v_m$ ) with parameters  $\mu = v_m = 1.18$  m/s and  $\sigma/\mu = 0.167$  (Nash–Sutcliffe coefficient 0.82); and (b) accounting for the dip-phenomenon (optimum  $h/d = 0.1$ ) by the Chiu (1988) model with parameters  $v_m = 1.14$  m/s and  $M = 2$  (Nash–Sutcliffe coefficient 0.1), optimum  $M = 3.2$  (Nash–Sutcliffe coefficient 0.69) and  $M = 4$  (Nash–Sutcliffe coefficient 0.57), and the ME2 model with parameters  $\mu = v_m = 1.17$  m/s and  $\sigma/\mu = 0.167$  (Nash–Sutcliffe coefficient 0.83).

### 3.4. Implications to sampling for streamflow estimation

In this section, we show some implications of the proposed framework to velocity sampling and streamflow estimation in a two-dimensional cross-section. The most common method to measure the flow velocity at a single point is to use a mechanical current meter; the first one was designed and built in 1882 by W.G. Price (WMO, 2010). The mechanical current meters contain a rotating element the angular velocity of which is proportional to the flow velocity. During the last decades, electronic current meters have also been made available. These are based either on the acoustic Doppler effect or on Faraday's law to obtain the flow velocity, and offer higher accuracy and convenience compared to the mechanical meters, though at a much higher price. Although one may employ different devices for the estimation of the discharge, the most common sampling practice is to point-sample the velocity field, assuming steady-state hydraulics and stable channel geometry (measurable with good accuracy over short times). Such a practice is tedious, often dangerous, and even infeasible under high flows (e.g., Sasso et al., 2018). Commonly these locations are selected at 20%, ~60% and 80% of the depth on a number of verticals (typically one vertical every 1 m or every 10% of the width for very wide sections). The selection of those locations is semi-empirical; it is guided by an idealised deterministic model, e.g. the von Kàrman logarithmic velocity profile of normal, turbulent flow in an infinitely wide channel.

Under the presented framework, the locations are also treated as random variables in natural cross-sections (even if they are a priori chosen as a percentage of the total depth), since the depth is not a priori known and is itself treated as a random variable. In fact, it is shown (Dimitriadis et al., 2019b) that the probability distribution of the location is axiomatically set and affects any integration of the regular and random variables within the proposed framework. It is also discussed how the aforementioned distribution can be viewed as the sampling location distribution with the convenient choice of the uniform distribution. We note that since the latter distribution is set by assumption, one may employ a different distribution, e.g., an exponential, where more points are sampled close to the channel bottom and fewer close to the surface. However, such a task would be more difficult, since the type of the distribution affects the Monte-Carlo integration (see details in Dimitriadis et al., 2019b, sect. 3.2), and therefore, the new distribution must be included in all calculations within the proposed framework (see discussion and expressions in Dimitriadis et al., 2019b, sect. 3.2). Also, this task may be even unnecessary, since the uniform distribution has a simpler expression and has certain practical merits. In particular, its density is independent to the water-depth, and therefore, no water-depth recording is required during a uniform sampling of velocities in a cross-section. In any case, one should not mix the above configurations, in the sense that if a uniform (or other) distribution is assumed then all calculations should be performed based on this distribution for the sampling locations.

In Fig. 9, we test the effect of the sampling distribution in a bend trapezoidal channel by comparing a nearly-uniform sampling (i.e. velocities are recorded in such a manner as to cover uniformly the whole section), with a far-from-uniform sampling by selecting only the velocities at depths 20%, 60% and 80% of the total depth measured from the water surface. We also observe that the velocity distribution is close-to-Gaussian ( $R^2 = 0.98$ ) in cases where a uniform sampling distribution is employed. Furthermore, in cases where the probability distribution of the sampling locations deviates from uniformity, the velocity probability distribution results in a more complicated form that cannot be easily recognized among commonly known distributions.

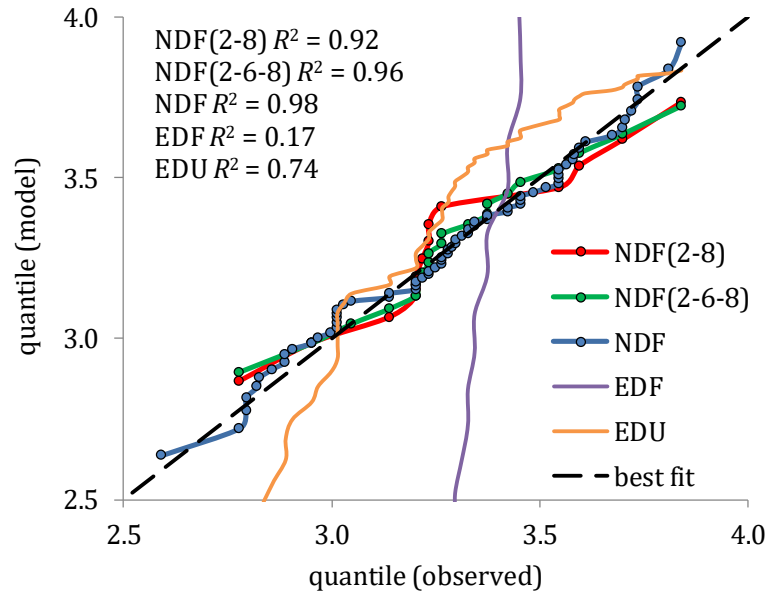


Figure 9: :Quantile-quantile test for the velocity measurements (data extracted graphically from Chiu, 1988, Fig. 9) for the Exponential Distribution Function (EDF), the exponential one truncated at a finite maximum velocity (EDU), and the Gaussian distributiun for the whole set of measurements (NDF), for sampling at 20%-60%-80% of the total depth (2-6-8), and at 20%-80% (2-8).

To further examine the implications of the number of samples in discharge estimation, we estimate the error from sampling smaller number of velocities again in a uniform manner. The error is calculated as the absolute difference between the simulated and true discharge divided by the true discharge (i.e. mean velocity from all available velocity samples). The standardized discharge error is estimated from 2 to 50 points (out of the available 68) selected in a uniformly random manner. For every set of points, we repeat the Monte-Carlo experiment for 1000 simulations. In Fig. 10, we plot the mean and standard deviation from all the standardized discharge errors. We observe that even with only 10 sampling points we may estimate the streamflow with a mean error less than 3% on average, and with a standard deviation of this error less than 2%.

It is noted that the river discharge can be estimated within a 10% accuracy if only the surface velocity is densely sampled (similar conclusions are drawn in other studies when accounting for other uncertainties in streamflow estimation in natural channels, e.g. Fulton and Ostrowski, 2008; Chen et al., 2013). In particular, after we fit the model based on the ME2 (as shown in Fig. 8 and 9), we simulate the surface velocities based on the ME2 profile (as shown and discussed in sect. 3.3), and we conduct a Monte-Carlo method based solely on the surface simulated velocities. We find that for a small sample (e.g., 2 to 10 points) the average error is similar (around 10%) but the standard deviation significantly decreases from 7% to 2%. However, as the sample of points increases the standard deviation of the error slightly decreases whereas the average error significantly increases. The latter behaviour is expected since the average velocity of the horizontal line at the surface has a much smaller average velocity around 1 m/s (compared to the simulated average of 1.17 m/s as shown in sect. 3.3 and Fig. 8). This effect will be investigated in future research, so as to find an optimum sampling location range at surface, from which the average of the surface velocities will be close to the average velocity of the whole cross-section.

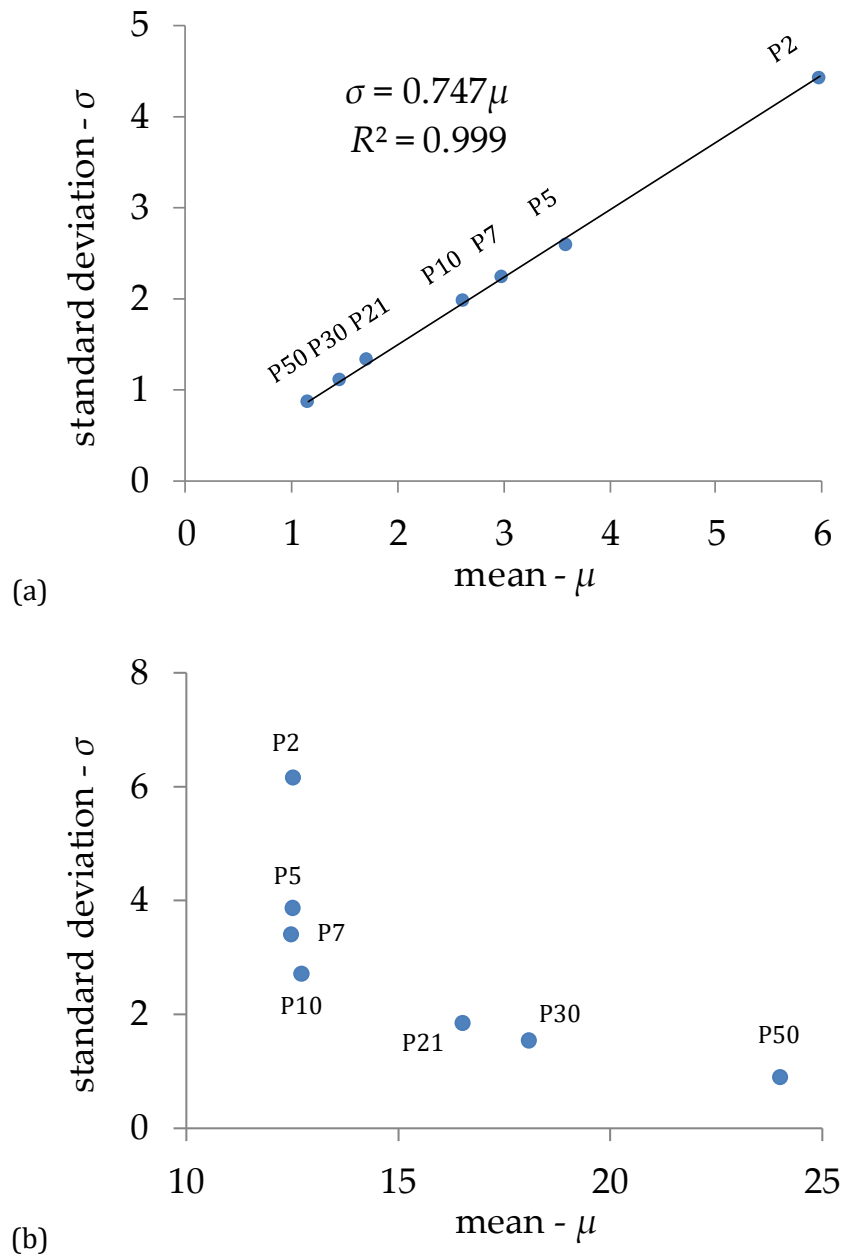


Figure 10: The expected average vs. standard deviation of the standardized error (in %) of the streamflow of a trapezoidal cross-section (data graphically obtained from Chiu, 1988, Fig. 9) for a range of points (2 to 50) randomly selected for 1000 set of experiments (a) from all the recorded velocities obtained by Yen (1965), and (b) from the simulated surface velocities along the whole width at the surface of the cross-section with distance between adjacent points equal to 5% of the total depth.

#### 4. Discussion and conclusions

In this study we apply the framework developed in Dimitriadis et al. (2019b), where we derive theoretical profiles for the longitudinal velocity, pressure and water-depth in natural cross-sections under one-dimensional steady flow dynamics and the revisited principle of maximum

entropy. The maximum entropy distribution is applied to each variable of interest based on the number of moments preserved through the 1d conservation of mass, linear momentum and energy. This distribution is then combined with the sampling location distribution, which for convenience is assumed uniform, to express the absolute derivative of the variable of interest with respect to location.

Through numerous applications, we illustrate how the proposed framework may be more flexible than the established one, as well as more consistent, in the sense that there is no need to introduce additional parameters to explicitly simulate specific flow conditions, such as the open-channel dip-phenomenon or turbulent pipe flow. By applying several assumptions, after we express the absolute derivative through the presented framework such as the behaviour of the shear stress, we may implicitly simulate the location and magnitude of the maximum velocity in a cross-section. We particularly show that such phenomena can be generated by the probability distribution of the velocity through the parameters related to variance and skewness. An important and practical advantage for open-channel flows is that if we know the velocity distribution and the Boussinesq and Coriolis parameters, and we measure the maximum depth and surface velocities, which can be both sampled by non-invasive methods, the mean velocity can be well approximated based on the proposed model, and thus, the streamflow of the cross-section. In the case of pipe-flows, instead of the maximum depth, which is fixed based on the geometry (e.g. at the pipe radius for circular section), and the velocities at the boundaries, which are set based on the boundary conditions (e.g. zero for the no-slip condition), we require the velocity magnitude in any selected location within the cross-section as well as the Boussinesq parameter in case of symmetrical geometries or additionally the Coriolis parameter, which both can be assumed fixed (a reasonable assumption for known geometry, roughness and flow conditions, e.g. turbulent) or can be implicitly simulated through empirical formulas.

We further illustrate how the assumed uniform distribution for the location variable can be regarded as the spatial sampling distribution in a cross-section, and that if one employs a different distribution, the framework must be accordingly adjusted to avoid inconsistencies and mis-evaluations. Although one may employ a different sampling distribution, the uniform one (i.e. uniformly random selection of points) requires the least sampling effort for the recorded information in a fixed area (e.g., no need to record depth during a uniform velocity sampling). Finally, we show that even with a few velocity samples (10 samples for the examined case in section 3.4), we may estimate the streamflow with a small error on average (less than 3%), and with a small standard deviation of this error (less than 2%), as well as with a relatively high accuracy (10%) if only surface velocities are sampled.

## **Acknowledgements**

The authors acknowledge the funding from the Hellenic General Secretariat for Research & Technology, under the National Strategic Reference Framework (2014-2020), for the project HYDRO-NET: Hydro-Telemetric Networks of Surface Waters: Gauging instruments, smart technologies, installation and operation, as a part of the Hellenic Integrated Marine and Inland Water Observing, Forecasting and Offshore Technology System, HIMIOFoTS (MIS5002739).

## **References**

Araujo, J.C., and Chaudhry, F.H., Experimental evaluation of 2-D entropy model for open-channel

flow, *J. Hydraul. Eng.*, 124(10),1064–1067, 1998.

Barbe, D.E., Cruise, J.F., and Singh, V.P., Solution of three-constraint entropy-based velocity distribution, *J. Hydraul. Eng.*,117(10), 1389–1396, 1991.

Barbe D.E., Cruise J.F., Singh V.P., *Derivation of a Distribution for the Piezometric Head in Groundwater Flow Using Entropy*, In: Hipel K.W. (eds) Stochastic and Statistical Methods in Hydrology and Environmental Engineering. Water Science and Technology Library, vol 10/4. Springer, Dordrecht, 1994.

Bechle, A. J., and C.H. Wu, An entropy-based surface velocity method for estuarine discharge measurement, *Water Resour. Res.*,50,6106–6128, doi:10.1002/2014WR015353, 2014.

Bogue, D.C. and A.B. Metzner, Velocity Profiles in Turbulent Pipe Flow -Newtonian and Non-Newtonian Fluids, *Industrial & Engineering Chemistry Fundamentals*, 2, 143, 1963.

Case, K.M., *Physics of Fluids*, 3, 149, 1960.

Castro, O.O., and W.H. Hager, *Non-Hydrostatic Free Surface Flows*, Advances in Geophysical and Environmental Mechanics and Mathematics Book Series, Springer: New York, NY, USA, 2017.

Chen, Y. C., and C. L. Chiu, An efficient method of discharge measurement in tidal streams, *J. Hydrol.*, 265(1–4), 212–224, 2002.

Chen, Y.C., and C.L. Chiu, A fast method of flood discharge estimation, *Hydrol. Processes*,18, 1671–1684, 2004.

Chen, Y.C., and S.P. Kao, Velocity distribution in open channels with submerged aquatic plant, *Hydrol. Processes*, 25(13), 2009–2017, 2011.

Chen, Y. C., Yang, T. M., Hsu, N. S., and Kuo, T. M., Real-time discharge measurement in tidal streams by an index velocity, *Environ. Monit. Assess.*, 184(10), 6423–6436, 2012.

Chen, Y.C.; Hsu, Y.C.; Kuo, K.T., Uncertainties in the Methods of Flood Discharge Measurement, *Water Resour. Manag.*, 27, 153–167, 2013.

Chiu C.L., Application of Probability and Entropy Concepts in Hydraulics, *Journal of Hydraulic Engineering*, 113: 583-599, 1987.

Chiu, C.L., Entropy and 2-D velocity distribution in open channels, *J. Hydr. Engrg.*, ASCE, 114(7), 738-756, 1988.

Chiu, C.L., Velocity distribution in open channel flow, *J. Hydraul. Engng.*,115, 576-594, 1989.

Chiu, C.L., Application of entropy concept in open channel flow study, *J. Hydr. Engrg.*, ASCE, 117(5), 615-628, 1991.

Chiu, C.L. and Murray, D.W., Variation of velocity distribution along nonuniform open-channel flow, *J. Hydraul. Engng.*, 118(1), 989-1001, 1992.

Chiu, C.L. and Said, C.A., Maximum and mean velocities and entropy in open-channel flow, *J. Hydraul. Engng.*, 121(1), 26-35, 1995.

Chiu, C.L., and Tung, N.C., Maximum velocity and regularities in open-channel flow, *J. Hydraul. Eng.*,128(4), 390–398, 2002.

Chiu, C.-L., and S.-M. Hsu, Probabilistic approach to modeling of velocity distributions in fluid flows, *J. Hydrol.*,316, 28–42, 2006.

Chiu, C.-L., Lin, G.-F., and Lu, L.-M., Application of probability and entropy concepts in pipe-flow study. *J. Hydraul. Eng.*, 119(6),742–756, 1993.

Chiu, C.L., Hsu, S.M., and Tung, N.C., Efficient methods of discharge measurements in rivers and streams based on the probability concept, *Hydrol. Processes*, 19, 3935–3946, 2005.

- Choo, Y.M., G.S. Yun, T.H. Choo, Y.B. Kwon, and S.Y. Sim, Study of shear stress in laminar pipe flow using entropy concept, *Environmental Earth Sciences*, 76(17), 616, 2017.
- Cui, H., and Singh, V.P., Two dimensional velocity distribution in open channels using Tsallis entropy, *J. Hydrol. Eng.*, 18(3), 331–339, 2013.
- Cui, H., and Singh, V.P., One dimensional velocity distribution in open channels using Tsallis entropy, *J. Hydrol. Eng.*, 19(2), 290–298, 2014.
- Dingman, S. L., Probability distribution of velocity in natural channel cross-sections, *Water Resour. Res.*, 25(3), 509–518, 1989.
- Dimitriadis, P., A.D. Koussis, N. Kappos, D. Katsanos, S. Lykoudis, K. Mazi, and E. Rozos, Entropy-maximization method of discharge determination revisited: a stochastic-deterministic framework for estimating spatial velocity profiles in open-channel flow and its implications for sampling, *European Geoscience Union General Assembly*, EGU2019-15259, Vol. 21, 2019a.
- Dimitriadis, P., A.D. Koussis, D. Koutsoyiannis, Estimating the hydraulic profiles of velocity, pressure and depth in natural cross-sections by employing the entropy maximization principle under one-dimensional steady-flow dynamics: I. Theoretical concepts, 2019b (submitted).
- Farina, G., S. Alvisi, M. Franchini, T. Moramarco, Three methods for estimating the entropy parameter M based on a decreasing number of velocity measurements in a river cross-section, *Entropy*, 16 (5), 5222512–2529, 2014.
- Farina, G., Alvisi, S., Franchini, M., Corato, G., Moramarco, T., Estimation of bathymetry (and discharge) in natural river cross-sections by using an entropy approach, *J. Hydrol.*, 527, 20–29, 2015.
- Felder, S., and H. Chanson, Free-surface profiles, velocity and pressure distributions on a broad-crested weir: A physical study, *J. Irrig. Drain. Eng.*, 138(12), 1068–1074, 2012.
- Fontana, N., G. Marini, and F. De Paola, Experimental assessment of a 2-D entropy-based model for velocity distribution in open channel flow, *Entropy*, 15, 988–998, doi:10.3390/e15030988, 2013.
- Fulton, J., and J. Ostrowski, Measuring real-time streamflow using emerging technologies: Radar, hydroacoustics, and the probability concept, *J. Hydrol.*, 357(1), 1–10, 2008.
- Greco, M., Effect of bed roughness on 1-D entropy velocity distribution in open channel flow, *Hydrol. Res.*, 46, 1–10, 2015.
- Greco, M., Entropy-based approach for rating curve assessment in rough and smooth irrigation ditches, *J. Irrig. Drain Eng.*, 142, 04015062, 2016.
- Greco, M., and Mirauda, D., Entropy parameter estimation in large-scale roughness open channel, *J. Hydrol. Eng.*, 20, 2015.
- Greco, M., and Moramarco, T., Influence of bed roughness and cross-section geometry on medium and maximum velocity ratio in open-channel flow, *J. Hydraul. Eng.*, 10, 2015.
- Greco, M., Mirauda, D., Plantamura Volpe, A., Manning's roughness through the entropy parameter for steady open channel flows in low submergence, *Procedia Eng.*, 70, 773–780, 2014.
- Guo, J., and Julien, Y.P., Shear stress in Smooth Rectangular Open Channel Flows, 131:1(30), 2005.
- Hervouet, J.M., Solving non-hydrostatic Navier–Stokes equations with a free surface, in: Brebbia, C.A. (Ed.), *Coastal Engineering VI*, WIT Press, Southampton, Boston, pp. 3–22, 2003.
- Jiang, Y.; Bin, L.; Chen, J., Analysis of the Velocity Distribution in Partially-Filled Circular Pipe Employing the Principle of Maximum Entropy, *PloS ONE*, 11, 1-17, 2016.
- Khoo, B.C., Y.T. Chew, and C.J. Teo, On near-wall hot-wire measurements, *Exp. Fluids*, 29, 448, 2000.
- Kazemian, K.K., H. Bonakdari, A. Gholami, Z.S. Khozani, A.A. Akhtari, and B. Gharabaghi,

Uncertainty analysis of shear stress estimation in circular channels by Tsallis entropy, *Physica A: Statistical Mechanics and its Applications*, 510, 558-576, 2018.

Kazemian K.K.A., H. Bonakdaria, A. Gholamia and B. Gharabaghlib, The uncertainty of the Shannon entropy model for shear stress distribution in circular channels, *International Journal of Sediment Research*, 2019.

Khozani, Z.S.; and Bonakdari, H., Formulating the shear stress distribution in circular open channels based on the Renyi entropy, *Physica A*, 490, 114–126, 2018.

Koussis, A., Akylas, E., and Mazi, K.: Response of sloping unconfined aquifer to stage changes in adjacent stream II, Applications, *J. Hydrol.*, 338, 73–84, doi:10.1016/j.jhydrol.2007.02.030, 2007.

Kumbhakar, M., K. Ghoshal, Two dimensional velocity distribution in open channels using Renyi entropy, *J. Physica A.*, 450, 546-559, 2016.

Kumbhakar, M., K. Ghoshal, and V.P. Singh, Two-dimensional distribution of streamwise velocity in open channel flow using maximum entropy principle: incorporation of additional constraints based on conservation laws, 2019a (submitted).

Kumbhakar, M., K.R. Ray, S.K. Chakraborty, K. Ghoshal, and V.P. Singh, Mathematical Modelling of Streamwise Velocity Profile in Open Channels Using Tsallis Entropy, *Computational Physics*, arXiv:1910.12534, 2019b (submitted).

Kumbhakar, M., K.R. Ray, S.K. Chakraborty, K. Ghoshal, and V.P. Singh, On the Role of Tsallis Entropy Index for Velocity Modelling in Open Channels, *Computational Physics*, arXiv:1910.11665, 2019c (submitted).

Maghrebi, M.F., and M. Rahimpour, A simple model for estimation of dimensionless isovel contours in open channels, *Flow Meas. Instrum.*, 16, 347–352, 2005.

Maghrebi M.F., and M. Rahimpour, Streamwise velocity distribution in irregular shaped channels having composite bed roughness, *J. Flow Meas Instrum.*, 17:237–245, 2006.

Marini, G., Martino, G. D., Fontana, N., Fiorentino, M., and Singh, V. P., Entropy approach for 2D velocity distribution in open channel flow, *J. Hydraul. Res.*, 49(6), 784–790, 2011.

Marini, G., Fontana, N., and Singh, V.P., Derivation of 2D velocity distribution in watercourses using entropy, *Journal of Hydrologic Engineering*, 22(6), 2017.

Mead L.R., and N. Papanicolaou, Maximum entropy in the problem of moments, *Journal of Mathematical Physics*, 25(8): 2404–2417, 1984.

Mirauda, D., Pannone, M., and De Vincenzo, A., An entropic model for the assessment of streamwise velocity dip in wide open channels, *Entropy*, 20, 69, 2018.

Mohamed, H.I., Identification of Pressure and Velocity Correction Coefficients along Block-Stone Ramp, *8th. International Water technology Conf.*, IWTC8 2004, Alexandria, Egypt, 2004.

Moramarco, T., Saltalippi, C., and Singh, V. P., Estimating the cross-sectional mean velocity in natural channels using Chiu's velocity distribution, *J. Hydrol. Eng.*, 9(1), 42–50, 2004.

Moramarco, T.; Corato, G.; Melone, F.; Singh, V.P., An entropy-based method for determining the flow depth distribution in natural channels, *J. Hydrol.*, 497, 176–188, 2013.

Moramarco, T.; Barbetta, S.; Tarpanelli, A. From surface flow velocity measurements to discharge assessment by the entropy theory, *Water*, 9, 120, 2017.

Moramarco, T., S. Barbetta, D.M. Bjerklie, J.W. Fulton and A. Tarpanelli, River Bathymetry Estimate and Discharge Assessment from Remote Sensing, *Water Resources Research*, 2019.

Naghavi, B., K. Esmaili, J. Yazdi, and F.K. Vahid, An experimental and numerical study on hydraulic characteristics and theoretical equations of circular weirs, *Canadian Journal of Civil Engineering*,

38(12): 1327–1334. doi: 10.1139/l11-092, 2011.

Papadimitrakis, I.A., and Orphanos, I., Statistical analysis of river characteristics in Greece, basic hydraulic parameters, *Hydrological Sciences Journal*, Vol. 54, Issue 6, pp. 1035-1052, 2009.

Peppas, M.V., Application of geostatistical interpolation methods for estimating the mean velocity in a trapezoidal cross-section, MSc thesis, 91 pages, Athens, October 2008.

Perks, M.T., S. Dal, A. Hauet, C. Le, S. Pearce, S. Peña-Haro, F. Tauro, S. Grimaldi, B. Hortobágyi, M. Jodeau, I. Maddock, L. Pénard, and S. Manfreda, Towards harmonization of image velocimetry techniques for river surface velocity observations, *Earth System Science Data*, 2019.

Pizarro, A., C. Samela, M. Fiorentino, O. Link, and S. Manfreda, BRISSENT: An Entropy-Based Model for Bridge-Pier Scour Estimation under Complex Hydraulic Scenarios, *Water*, 9, 889, 2017.

Rahimpour, M., Dimensionless isovelocity contours in rectangular cross-sections by harmonic mean distances, *ISH Journal of Hydraulic Engineering*, 2017.

Rockinger, M., and E. Jondeau, Entropy densities with an application to autoregressive conditional skewness and kurtosis, *J. Econ.*, 106, 119–142, 2002.

Rudman, M., L.J.W. Graham, H.M. Blackburn, L. Pullum, Non-Newtonian turbulent and transitional pipe flow, in the 15<sup>th</sup> International Conference on Hydrotransport: incorporating the 11th International Symposium of Freight Pipelines, Banff (Canada), BHR Group Limited, the Fluid Engineering Centre, 2002.

Sarma, K.V.N., B.V.R. Prasad, and A.K. Sarma, Detailed study of binary law for open channels, *J. Hydraul. Eng.*, 126(3), 210–214, 2000.

Santana, D., Rodriguez-Rodriguez, J., Almedros-Ibanez, J.A., Martinez-Bazan, C., Characteristics lengths and maximum entropy estimation from probe signals in the ellipsoidal bubble regime, *International Journal of Multiphase Flow*, 32, 1123–1139, 2006.

Sasso, F.D., A. Pizarro, C. Samela, L. Mita, and S. Manfreda, Exploring the optimal experimental setup for surface flow velocity measurements using PTVS, *Environ. Monit. Assess.*, 190:460, 2018.

Schlichting, H., and K. Gersten, *Boundary-layer theory*, Graduate Texts in Mathematics, Springer-Verlag, 2017.

Sheikh, Z., and H. Bonakdari, Prediction of boundary shear stress in circular and trapezoidal channels with entropy concept, *Urban Water Journal*, 13(6), 629-636, 2015.

Shannon, C.E., A Mathematical Theory of Communication, *The Bell System Technical Journal*, Vol. 27, Oct., pp. 623-656, 1948.

Singh, V.P., Derivation of furrow geometry using entropy theory, *Trans. ASABE*, 55(3), 987–993, 2012.

Singh, V.P., *Entropy theory in hydraulic engineering: an introduction*, American Society of Civil Engineers, 2014.

Singh, V.P., and Luo, H., Entropy theory for distribution of one-dimensional velocity in open channels, *J. Hydrologic Eng.*, 10.1061/(ASCE)HE.1943-5584.0000363, 725–735, 2011.

Singh, V.P., Marini, G., and Fontana, N., Derivation of 2D power-law velocity distribution using entropy theory, *Entropy*, 15, 1221–1231, 2013.

World Meteorological Organization, *Manual on stream gauging*, vol. I and II. WMO-No.1044, Geneva, Switzerland, 2010.

Wibowo, H., Manning Roughness Coefficient Study on Bed Materials Non-Cohesive with Parameters Using Entropy to Open Channel Flow, *Proceedings of International Conference: Issues, Management And Engineering In The Sustainable Development On Delta Areas Semarang*,

Indonesia – February 20th, 2015.

Winitzki, S., A handy approximation for the error function and its inverse, Lecture Note, 2008.

Xia, R., Relation between mean and maximum velocities in a natural river, *J. Hydraul. Eng.*, 123(8), 720–723, 1997.

Yang, S.Q.; Tan, S.K.; Lim, S.Y., Velocity distribution and dip-phenomenon in smooth uniform channel flows, *J. Hydraul. Eng.*, 130, 1179–1186, 2004.

Yang, S.Q.; Tan, S.K.; Wang, X.K., Mechanism of secondary currents in open channel flows, *Geophys. Res.*, 117, F04014, 2012.

Yen, B.C., Open-channel flow equations revisited, *J. Eng. Mech. Div., Am. Soc. Civ. Eng.*, 99(5), 979–1009, 1973.

Yoon, J.I., Sung, J., and Lee, M.H., Velocity profiles and friction coefficients in circular open channels, *Journal of Hydraulic Research*, 50:3, 304–311, doi:10.1080/00221686.2012.673745, 2012.

Yuan, H.L., and Wu, C.H., An implicit three-dimensional fully non-hydrostatic model for free-surface flows, *International Journal for Numerical Methods in Fluids*, 46(7), 709–733, 2004.

Zerihun, Y., A Non-Hydrostatic Depth-Averaged Model for Hydraulically Steep Free-Surface Flows, *Fluids*, 2(4):49, 2017.

Zhang, G., and H. Chanson, Hydraulics of the developing flow region of stepped spillways, II. Pressure and velocity fields, *J. Hydraul. Eng.*, 04016016, 2016.